J Nanostruct Chem (2016) 6:75–92
DOI 10.1007/s40097-015-0180-z

ORIGINAL RESEARCH

Photobiological synthesis of noble metal nanoparticles using *Hydrocotyle asiatica* and application as catalyst for the photodegradation of cationic dyes

Thangavel Akkini Devi[1] · Narayanan Ananthi[1] · Thomas Peter Amaladhas[1]

Received: 9 August 2015 / Accepted: 19 October 2015 / Published online: 14 November 2015

Abstract Solar light induced photo catalysis by plasmonic nanoparticles such as Au and Ag is an important field in green chemistry. In this study an environmental benign method was investigated for the rapid synthesis of colloidal Ag and AuNPs using the extract of *Hydrocotyle asiatica*, as a reducing and stabilizing agent under sunlight irradiation. The nanoparticles were formed in few seconds and were characterized by UV–Vis., FT-IR, TEM, EDAX, XRD, DLS and Zetasizer. The nanoparticles were stable in aqueous solution for more than 6 months. TEM analysis established that the Ag and AuNPs were predominantly spherical with average size of 21 and 8 nm, respectively. The flavonoids and glycosides from the extract of *H. asiatica* were proved to be responsible for the reduction and capping through FT-IR analysis. The antimicrobial studies of AgNPs showed effective inhibitory activity against the clinical strains of gram-negative and positive bacteria. The localized surface plasmon resonance of AgNPs was used for the photo-driven degradation of cationic dyes (malachite green and methylene blue). Thus, this green technique can be used for bulk production of AgNPs, and thus prepared nanoparticles may be used for removal of dyes from effluent.

Graphical Abstract

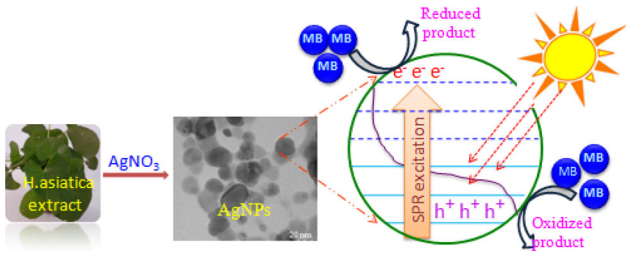

Keywords Biosynthesis · Silver and gold nanoparticles · *Hydrocotyle asiatica* · Malachite green · Methylene blue · Photobiological synthesis

Introduction

The essential of nanotechnology is to synthesize dispersed nanoparticles for potential applications in optics, biomedical sciences, drug delivery, catalysis and electronics. In the past, number of methods such as chemical [1–4], photochemical [5–8] and thermal [9, 10] have been developed to synthesize metallic nanoparticles. Recently an efficient method for fabrication of metallic nanoparticles from metallomicelles is reported [11]. Among these methods, photochemical method has gained considerable attention due to its convenience, but it employs toxic chemicals as reducing and stabilizing agent [12]. To avoid the utilization of highly toxic chemicals, the use of microorganisms and plant parts for nanoparticles synthesis has been explored [13]. Previous reports mention the use of microorganisms such as *Alternaria alternate* [14], and *Amylomyces rouxii* [15] for the synthesis of nanoparticles.

Electronic supplementary material The online version of this article (doi:10.1007/s40097-015-0180-z) contains supplementary material, which is available to authorized users.

✉ Thomas Peter Amaladhas
peteramaldhast@yahoo.co.in; peteramaladhas@gmail.com

Thangavel Akkini Devi
t.deviagni@gmail.com

Narayanan Ananthi
ananthi.red@gmail.com

[1] PG and Research Department of Chemistry, V.O. Chidambaram College, Tuticorin, Tamilnadu 628008, India

Recently, several plants extracts such as *Annona squamosa* [16], *Arbutus unedo* [17], *Cassia angustifolia* [18] and many others [19–27] have been used to synthesize silver (Ag) and gold (Au) nanoparticles (NPs). However, these natural sources, which have active ingredients, produce nanoparticles at slower rate. To overcome this, photo-assisted biosynthesis of Ag and AuNPs using many plants has been qualitatively investigated [28]. The sunlight irradiation technique has been formerly reported for the synthesis of nanoparticles using few plant materials such as *Allium sativum* [29], *Andrachnea chordifolia* [30], *Piper betle* [31], *Bacillus amyloliquefaciens* [32] and *Achyranthus aspera* [33]. Apart from plant materials, dendrimers and starch are also used as reducing/stabilizing agents in the sunlight-induced synthesis of nanoparticles [34, 35]. The nanoparticles produced by bio route have good stability due to the presence of capping agents like alkaloids, flavonoids and polyphenols, which are the major constituents present in the natural sources.

The localized surface plasmon resonance (LSPR) of noble metal nanoparticles makes them suitable for various applications. The surface plasmons live for few femto/picoseconds producing a shower of energetic electrons and holes and then dephase. By fabricating appropriately nanostructured materials that allow a reasonable fraction of these hot carriers to be harvested before they thermalize, the hot electrons can be transferred to appropriate catalyst systems and the material can be used to carry out light-enabled redox chemistry. Recently biosynthesized NPs have been reported to degrade organic dyes [36–42].

Hydrocotyle asiatica (Fig. 1) known as *Centella asiatica*, is a creeping perennial herbal plant with kidney-shaped leaves, found in India, Sri Lanka, Madagascar, South Africa, Australia, China, and Japan. *H. asiatica* is reported to contain triterpene acids (asiatic, madecassic acid, etc.), volatile and fatty oil (glycerides of palmitic acid, stearic, lignoceric, oleic, linoleic and linolenic acids), alkaloids (hydrocotylin), flavonoids (3-glucosylquercetin, 3-glucosylkaempferol and 7-glucosylkaempferol) and glycosides (asiaticoside A, asiaticoside B, madecassoside, etc.) [43]. The herb is well known for its high medicinal values; its antioxidant activity [44] and non-toxicity motivated us to carry out the present investigation.

Fig. 1 *Hydrocotyle asiatica* leaves

Dyes are synthetic organic compounds released as effluent by many industries producing paper, plastic, leather, food, cosmetic, textile and medicine. The use of synthetic complex organic dyes as coloring materials in textile industries has increased significantly. Dyes in general, azo dyes in particular are carcinogenic, affecting reproductive organs and develop toxicity and neurotoxicity. Therefore, the dyes are to be necessarily removed from industrial effluent before discharging into the natural sources. The dye effluents are highly resistant to microorganisms so that their reduction using conventional biological treatment is generally ineffective and also resistant to destruction by physical–chemical treatments in a high effluent concentration. Methylene Blue (MB) is one of the phenothiazine cationic dyes, used in coloring paper, dyeing cottons, wools and so on. It makes very harmful impacts on living things causing difficulties in breathing, vomiting, diarrhea and nausea [45]. Malachite Green (MG), a triphenylmethane dye is extensively used in the leather, paper, silk, cotton, and jute dyeing processes and also used as biocide in the global aquaculture industry treating protozoal and fungal infections.

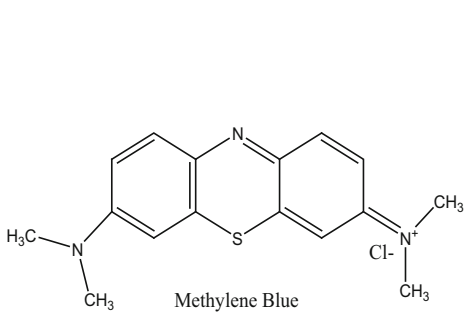

Methylene Blue

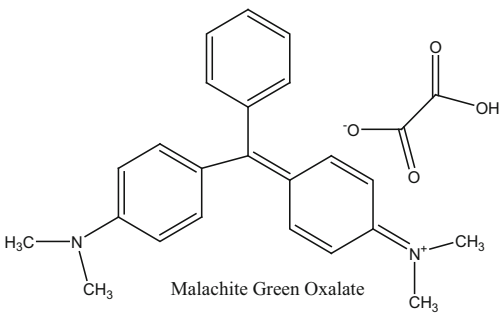

Malachite Green Oxalate

MG and its metabolites are known to cause mutagenic, carcinogenic, and teratogenic effects to living organisms [46]. Nanotechnology has been extended to the wastewater treatments in the recent years and due to high surface area, AgNPs exhibits an enhanced reactivity [47].

The present study deals with the biosynthesis of Ag and AuNPs in milligram quantities using abundantly available *H. asiatica* as a reducing and stabilizing agent. The kinetics of formation of Ag and AuNPs has been studied using Ultraviolet–Visible spectroscopy (UV–Vis) and the biosynthesized nanoparticles has been characterized using Transmission Electron Microscopy (TEM), Energy Dispersive X-ray Analysis (EDAX), X-ray Diffraction (XRD), Dynamic Light Scattering (DLS), Zetasizer and Fourier Transform Infra Red (FTIR) spectrometry. The potential applications of Ag and AuNPs as a catalyst for the photo degradation of two different cationic dyes, and as antibiotics have also been studied.

Materials and methods

Preparation of plant extract

The leaves of *H. asiatica* were collected from Eral, Tuticorin, Tamil Nadu, India. The plant was identified with the help of local flora and authenticated by botanical survey of India, Southern Circle, Coimbatore, Tamil Nadu, India. About 5 g of fresh leaves were washed thoroughly with tap water and finally with double distilled water and then cut into small pieces. These finely cut leaves were then boiled in 100 mL double distilled water in a 250 mL Erlenmeyer flask for a period of 5 min. After getting it cool, it was filtered through Whatman No. 41 filter paper. This clear filtrate was used for the synthesis of nanoparticles.

Biosynthesis of AgNPs

To make AgNPs, 5 mL of clear aqueous extract of *H. asiatica* was added to 10 mL of 10 mM $AgNO_3$ (Spectrochem, Mumbai, India, AR Grade) and 85 mL of double distilled water so as to make the final concentration to 1 mM. The solution mixture was then exposed to bright sunlight. The formation of AgNPs was observed by the appearance of yellowish brown color in 5 s and the periodic sampling was carried out to monitor the kinetics using UV–Vis. spectrophotometer. 1 mL of the aliquot was withdrawn from the reaction mixture and diluted to 10 mL with double distilled water before measuring the absorbance.

Biosynthesis of AuNPs

The aqueous extract of *H. asiatica* (2.0 mL) was added to 4.0 mL of 1 mM $HAuCl_4.3H_2O$ (Sigma-Aldrich, USA, 99.9 % purity) and the solution mixture was then exposed to bright sunlight. The formation of AuNPs was observed by the appearance of pinkish purple color in 45 s. The periodic sampling was carried out to monitor the kinetics of formation of AuNPs. For the UV–Vis spectral analysis, 1 mL of the aliquot was withdrawn from the reaction mixture and diluted to 5 mL with double distilled water.

Analysis of photo-bio reduced Ag and AuNPs

The UV–Vis spectral analysis was performed on a JASCO, V-530 spectrophotometer. FT-IR spectra for the dry powder (obtained by evaporation of leaves extract) and nanoparticles were recorded in the range of 4000–400 cm^{-1} with Thermoscientific, Nicolet iS5 spectrometer. TEM analysis was done on a PHILIPS, CM 200 instrument operated at 200 kV, resolution 2.4 Å. XRD measurements were carried out using a Panalytical X'Pert Powder X'Celerator Diffractometer, with CuKα monochromatic filter. EDX (JEOL Model JED-2300) analysis was used for identifying the elemental composition of Ag and AuNPs. Electrokinetic property (zeta potential) of NPs was evaluated using Zetasizer 1000 HS (Malvern Instruments, UK) at Defence Food Research Laboratory (DFRL), Mysore.

Assessment of antimicrobial activity

For antimicrobial study, 50 mL of as-prepared colloidal suspension of nanoparticles was centrifuged at 13,000 rpm for 15 min and the nanoparticles were dispersed in 1 mL double distilled water and used. Antimicrobial activity of the synthesized Ag and AuNPs was determined using the disc diffusion assay method on pathogenic strains of *Salmonella paratyphi*, *Pseudomonas aeruginosa*, *Streptococcus pyogenes* and *Streptococcus faecalis*. The test microbial suspensions were spread on Petri dishes and freshly prepared Ag and AuNPs samples were introduced. The control samples lacking the precursor were used to assess the antimicrobial activity of the extract. The samples were initially incubated for 15 min at 4 °C (to allow diffusion) and later on at 37 °C for 24 h for the culture. Positive test results were scored when a zone of inhibition was observed around the well after the incubation period. The diameter of zones of inhibition was measured using a meter ruler, and the mean value for each organism was recorded and expressed in millimeter.

Evaluation of photo degradation of cationic dyes by AgNPs

To prepare the AgNPs in solid form, the colloidal solution was centrifuged at 13,000 rpm for 15 min and the pellet

was washed with double distilled water to remove the excess biomolecules that were not capped and the washings were repeated for three times. The samples were dried at 60 °C, grounded and used for the degradation studies. 10 mg of AgNPs was added to 100 mL solution of 1×10^{-5} M methylene blue trihydrate (EMerck, Germany, Microscopy Grade) or malachite green oxalate (Spectrochem, Mumbai, Microscopy Grade) and the beaker was then exposed to sunlight with constant stirring using magnetic stirrer. To monitor the reaction, aliquots were withdrawn at predetermined time period and the suspension was centrifuged and the absorbance of the supernatant was subsequently measured using UV–Vis spectrophotometer.

Results and discussion

UV–Vis spectra of AgNPs

AgNPs are formed by the sunlight-induced reduction of Ag^+ ions by the addition of leaf extract. The colorless solution turned reddish brown, in 5 s of exposure to sunlight, indicating the formation of AgNPs. The formation of AgNPs is monitored using UV–Vis spectrophotometer in the range of 200–800 nm, where an intense peak was obtained at 436 nm, which is known as Localized Surface Plasmon Resonance (LSPR) band due to the excitation of free electrons in the nanoparticles. The peak is sharp and symmetrical in shape signifying the formation of mono dispersed AgNPs [33].

Figure 2a represents the UV–Vis spectra of synthesized AgNPs as a function of interaction time. From the figure it is evident that the formation of AgNPs mainly depends on the time of exposure to sunlight. It can be observed that the absorbance is increased with exposure time (Fig. 2b), indicating more Ag^+ ions are reduced with time. Initially the absorbance of the solution increases exponentially after that it tends to attain almost a constant value indicating the completion of the reaction. By monitoring the LSPR band from 0 to 55 min, it can be seen that there is a blue shift of λ_{max} from 441 to 411 nm with the consequent color changes from reddish brown to yellow. This kind of blue shift is being reported to be due to the formation of small-sized nanoparticles [48] and narrowing of peak with time implies monodispersed AgNPs are formed with time and about 30 min may be taken as appropriate to get uniform-sized nanoparticles.

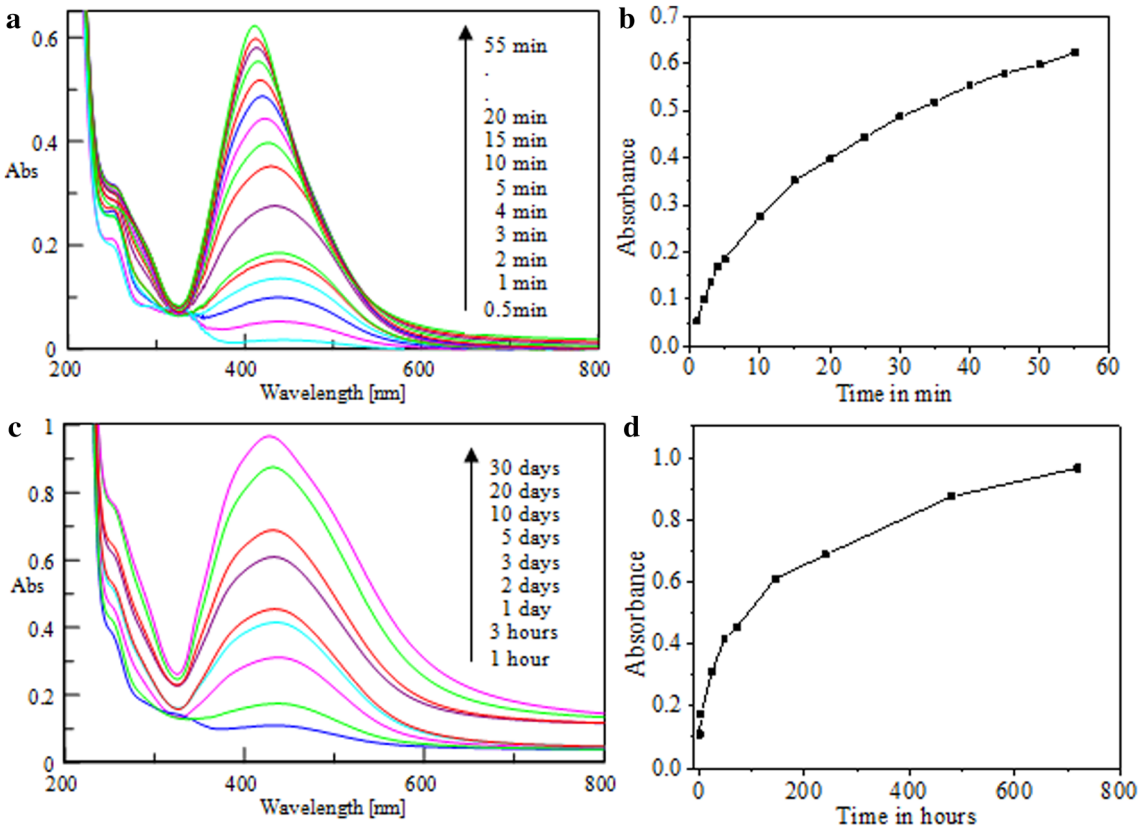

Fig. 2 UV–Vis spectra recorded as a function of time of reaction of *H. asiatica* extract with an aqueous solution of 1 mM $AgNO_3$: **a**, **c** presence and absence of sunlight, **b**, **d** variation of absorbance with time (presence and absence of sunlight)

For comparison, the title reaction is also studied at ambient conditions in the absence of sunlight. The reaction is slow and the appearance of yellowish brown color is noticed only after an hour, thereafter the color intensified slowly with time (Fig. 2c). The maximum absorption is observed at 437 nm and the LSPR band is broad signifying the poly-dispersed nature of nanoparticles. Initially the intensity increased almost linearly up to 6 days after that it tends to attain a maximum value (Fig. 2d) indicating the completion of reaction. It is observed that the λ_{max} is blue shifted from 437 nm to 428 nm with increase of reaction time from 1 to 30 days. The AgNPs are observed to be stable in solution for more than 1 month.

Effect of the synthesis variables on AgNPs

The effect of extract quantity, silver nitrate concentration, temperature and pH on the formation of AgNPs in the presence and absence of sunlight is also studied.

UV–Vis spectra of AgNPs synthesized in presence of sunlight

Effect of volume of extract

The volume of the extract was varied from 1 to 3 mL by keeping the $AgNO_3$ concentration constant. From Figure S1 (S—Supporting Materials), it is observed that initially the absorbance of LSPR band increases and then decreases. Minimum volume of leaf extract is preferred to have stable AgNPs.

Effect of $AgNO_3$ concentration

The $AgNO_3$ concentration was varied from 1 to 10 mM, while keeping the extract volume constant. On increasing the concentration of silver nitrate, the formation of NPs is also increased linearly up to 7 mM after that it tends to attain maximum value. There is no appreciable shift in the λ_{max} is observed (Figure S2).

Effect of pH

To study the effect of pH, extract pH was adjusted to 3–11 by adding 0.1 M sulphuric acid or 0.1 M sodium hydroxide. In all the pH ranges, the LSPR band appears between 411 and 429 nm indicating that there is no change in the shape of the NPs with change in pH (Figure S3). However, in alkaline pH (>9) the intensity of SPR band increases appreciably with a blue shift. This trend is reported earlier also signifying the formation of large amount of AgNPs and the blue shift is attributed to formation of small-sized nanoparticles [17].

UV–Vis spectra of AgNPs synthesized in absence of sunlight

Effect of volume of extract

The volume of extract was varied from 0.5 to 2.5 mL with 25 mL of 1 mM $AgNO_3$ solution. The spectrum was recorded after 24 h of reaction. Figure S4a represents the UV–Vis spectra of AgNPs synthesized using *H. asiatica* at different extract volume. At higher volume of extract, SPR peaks are broad indicating that the AgNPs are poly-dispersed. The red shift in the absorption maximum shows the aggregation of nanoparticles leading to larger particle size. For the generation of small AgNPs, minimum quantity of leaf extract is preferred. It is observed that initially the absorbance of SPR band increases while increasing the quantity of extract; at higher volumes it tends to attain a constant value (Figure S4b).

Effect of $AgNO_3$ concentration

The $AgNO_3$ concentration was varied from 1 to 3 mM, while keeping the extract volume constant. Figure S5a represents UV–Vis spectra of AgNPs prepared using *H. asiatica* at different $AgNO_3$ concentration. On increasing the concentration of $AgNO_3$, the formation of NPs is also increased up to 2.5 mM after that there is no change in absorbance (Figure S5b). There is a shift in the λ_{max} from 449 to 443 nm when the concentration of $AgNO_3$ is increased from 1.5 to 3.0 mM indicating the aggregation of NPs. On adding extract to higher concentration of $AgNO_3$ (4 and 5 mM), a black colored suspension is formed, may be due to the formation of silver oxide.

Effect of pH

To study the effect of pH, extract pH was adjusted to 2, 3, 4, 6 and 9 and then the extract (5 mL) was added to 95 mL of 1 mM silver nitrate solution to make the total volume to 100 mL. The spectrum was recorded after 24 h of reaction. Figure S6 represents UV–Vis spectra of AgNPs synthesized using *H. asiatica* at different pH values. At lower pH 2, 3 and 4, rate of formation of AgNPs is very slow when compared to pH 6. The broad SPR bands observed at lower pH values are due to large anisotropic particles. At higher pH 9, rate of formation of AgNPs is high. This may be due

to the large number of free functional groups available for silver binding, which facilitated higher number of silver ions to bind and subsequently form a large number of NPs with smaller diameters (λ_{max} 417 nm) [33].

Effect of temperature

To study the effect of temperature on AgNPs formation, the reaction was carried out at 35, 60, 80 and 100 °C in a water bath. The spectra were recorded after 1 h of reaction. As the temperature is increased, the rate of formation of AgNPs is also increased indicated by increase in the absorbance. Figure S7 represents UV–Vis spectra of AgNPs synthesized using *H. asiatica* at different temperature. At 35 °C, a broad SPR band indicates the formation of poly-dispersed AgNPs. With increase in the reaction temperature, the SPR band becomes narrow signifying the monodispersed nature of NPs. The λ_{max} of SPR band is shifted from 436 to 406 nm, due to the reduction in size of the NPs. With the increase of temperature from 35 to 80 °C more and more AgNPs are formed, after that not much increase is observed indicating the completion of the reaction.

All these results indicate the superiority of light induced method. More stable AgNPs are formed with uniform size distribution as implied by the sharp and narrow peaks in light reaction as compared to room temperature reaction. The rate of formation of nanoparticles is also very high in light reaction (min. vs days). As mentioned below the glycosides and flavonoids may act as reducing agents to reduce Ag^+ to AgNPs, the enhanced rate of reduction in the light irradiated reaction may be due to readily available electrons from the excitations of low energy transitions like π-π* in the biomolecules.

UV–Vis spectra of AuNPs

UV–Vis spectra of AuNPs formed by *H. asiatica* extract in bright sunlight at different reaction time are given in Fig. 3. Initially the reaction mixture was colorless, after exposing to sunlight the color of the reaction mixture changed to dark purple in 45 s. The broad band observed initially at 556 nm is changed to sharp peaks with time with the increase of absorption intensity till 40 min with a noticeable blue shift in absorption band. This observation indicates an increase in percentage of nanoparticles in solution and decrease in size with time. However, the absorption intensity of solution slowly decreases after 40 min, which may be due to change in the dimension of anisotropic nanostructures [49]. Hence, 30 min is considered to be optimal time to get monodispersed AuNPs. For comparison formation of AuNPs is also studied in the absence of sunlight, but the reaction is very slow and the AuNPs got aggregated to give a blue precipitate with time hence the reaction is not studied further.

FT-IR studies

FT-IR measurements are carried out to identify the possible bio components in *H. asiatica* leaf extract, which are responsible for stabilization of Ag and AuNPs. The FT-IR spectra of leaf extract and Ag and AuNPs are represented in Fig. 4. The untreated leaves extract shows prominent absorption bands at 3413, 2927, 1630, 1450, 1383, 1272

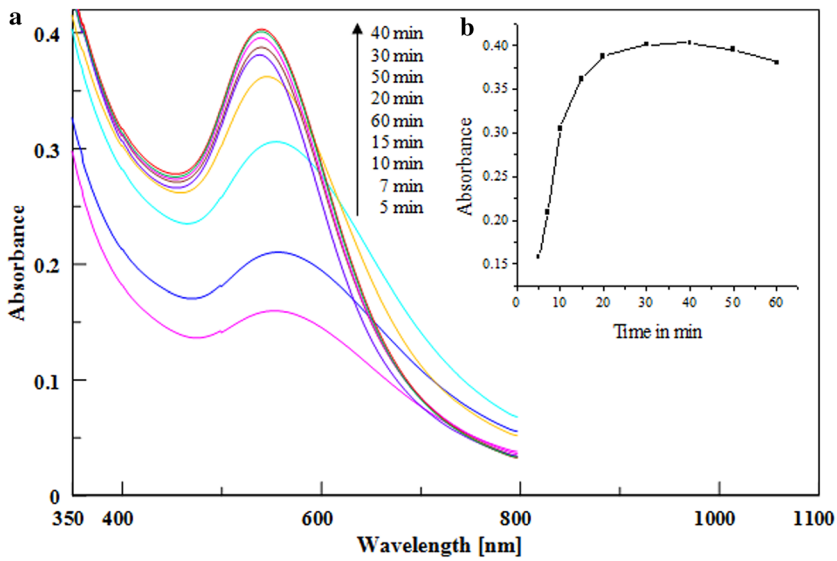

Fig. 3 **a** UV–Vis spectra recorded as a function of time of *H. asiatica* extract with an aqueous solution of 1 mM $HAuCl_4$ solution in sunlight, **b** variation of absorbance with time

and 1099 cm^{-1} (Fig. 4c). In the IR spectra, intense bands are observed at 3438, 2922, 1617, 1384 and 1097 cm^{-1} (Fig. 4b) and at 3451, 2923, 1629, 1384 and 1097 cm^{-1} (Fig. 4a) for Ag and AuNPs, respectively. Both spectra are almost identical indicating that the biomolecules responsible for stabilization are the same. The bands around 3400 cm^{-1} are due to alcoholic –OH stretching vibration, peak around 1630 cm^{-1} may be due to stretching vibrations of –C=C/–C=O, and the peak at 1384 cm^{-1} is probably due to –CH bending mode and the peak around 1099 cm^{-1} may be attributed to –C–O stretching vibration. The vibrational bands matching to the functional groups such as –OH, –C=O, –C=C and –C–O are probably derived from the water-soluble flavonoids and glycosides [50]. The presence of flavonoids in the extract was confirmed by Ferric chloride test (the extract when treated with few drops of Ferric chloride solution changed to blackish red color) and glycosides was confirmed by the Keller Killiani Test (the extract was treated with few drops of glacial acetic acid and Ferric chloride solution, mixed and concentrated sulphuric acid was added, lower reddish brown layer and upper acetic acid layer which turned bluish green indicated the presence of glycosides) [51]. The structures of important biomolecules present in *H. asiatica* leaves are given below.

TEM analysis

The morphology and size of the prepared Ag and AuNPs are analyzed by recording TEM images. TEM images of the Ag and AuNPs at different magnification are presented in Figs. 5 and 6 respectively. The TEM images clearly show that the nanoparticles are predominantly spherical in shape. The size is in the range of 6.6–33.6 and 8–35 nm for AgNPs in the presence, and absence of sunlight, respectively, and 5.2–10.3 nm for AuNPs in presence of sunlight. Figures 5i and 6f show the SAED pattern (circular ring) of Ag and AuNPs that revealed the polycrystalline nature of nanoparticles. The diffraction rings can be indexed on the basis of the fcc structure of Ag and AuNPs. Four rings arise due to reflections from (111), (200), (220) and (311) lattice planes of fcc of Ag and Au, respectively. This is further supported by broad Bragg's reflection observed in the XRD spectra.

EDAX analysis

EDAX analysis is carried out to confirm the elemental form of Ag and Au. The strong optical absorption peak is observed in the region of 3 keV (Fig. 7a) and 2 keV (Fig. 7b), which is typical for the absorption of metallic Ag

Glycosides

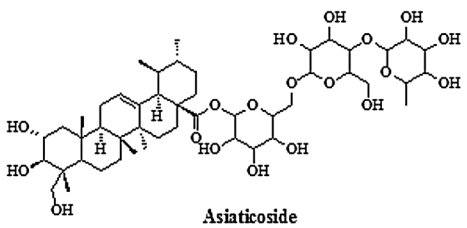

Asiaticoside

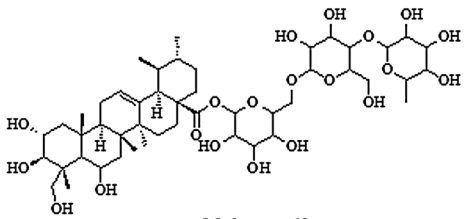

Madecassoside

Flavonoids

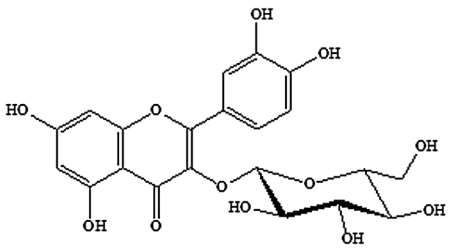

3-glucosylquercetin

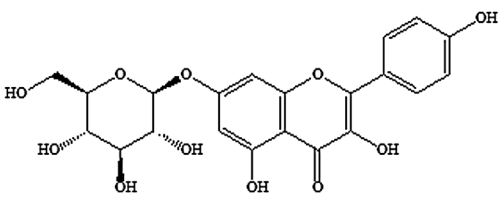

7-glucosylkaempferol

The peak at 1630 cm^{-1} is shifted to 1617 cm^{-1} in the case of AgNPs indicating the involvement of flavonoids or glycosides containing C=O groups in the stabilization of AgNPs.

[52] and Au [53] nanocrystallites, respectively. In addition to Ag and Au, peaks due to carbon and oxygen are also present, which further support the stabilization of nanoparticles by biomolecules.

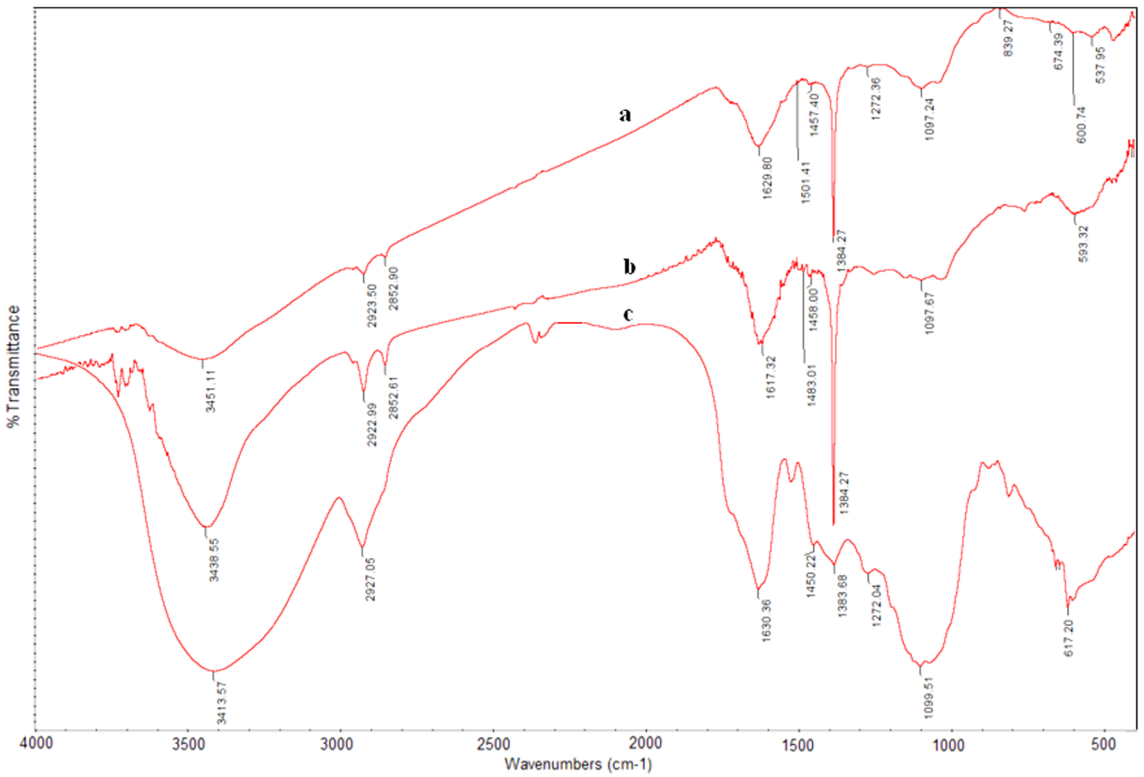

Fig. 4 FT-IR spectra of *a* Solid AuNPs, *b* Solid AgNPs and *c* dry powder obtained from the aqueous extract of *H. asiatica*

XRD studies

The powder X-ray diffraction patterns of the Ag and AuNPs are shown in Fig. 8a, b, respectively. XRD pattern of pure crystalline face-centered cubic (fcc) Ag has been published by the Joint Committee on Powder Diffraction Standards (JCPDS-2 4-0738). A comparison of XRD spectrum with the standard, confirm the crystalline nature of AgNPs, as evidenced by the peaks at 2θ values of 38.04°, 46.15°, 67.33° and 76.71°, corresponding to 111, 200, 220 and 311 planes, respectively. Similar peaks are obtained for the nanoparticles prepared in absence of light also.

The AuNPs show similar characteristic peaks of metallic fcc Au (JCPDS: 4-0784). The particle sizes of Ag and AuNPs are calculated by Debye–Scherrer Eq. (1) and the average sizes are found to be 17.26 and 12.84 nm, respectively.

$$D = k\lambda/\beta\cos\theta \quad (1)$$

where, k is the Scherrer constant, λ is the wavelength of the X-ray, β and θ are the half width of the peak and half of the Bragg angle, respectively.

In comparison to AgNPs, broad peaks are obtained in the XRD spectrum of AuNPs. Generally smaller-sized particles show peak broadening in the XRD pattern [54]. Broad peaks obtained in AuNPs are due to their smaller size. TEM results further augment this statement as smaller-sized AuNPs (8 nm) are produced in comparison to AgNPs (21 nm).

DLS and zeta potential studies

The data of DLS studies show that the average size of the AgNPs (Fig. 9a) is 53.64 nm and AuNPs (Fig. 9c) is 18.49 nm and the polydispersity index (PDI) is 0.245 and 0.330 for Ag and AuNPs, respectively, indicating moderate uniformity in the distribution of particles. The value of zeta potential of AgNPs (Fig. 9b) is −34.9 mV and AuNPs (Fig. 9d) is −20.7 with a single peak indicate the moderate repulsion between the nanoparticles. If the particles have a large negative zeta potential or large positive zeta potential, they will tend to repel each other and there will be no attraction to assemble together.

Antimicrobial studies

The antimicrobial activity of Ag and AuNPs is evaluated against various pathogenic strains including Gram-positive, Gram-negative bacteria. Generally, the antimicrobial

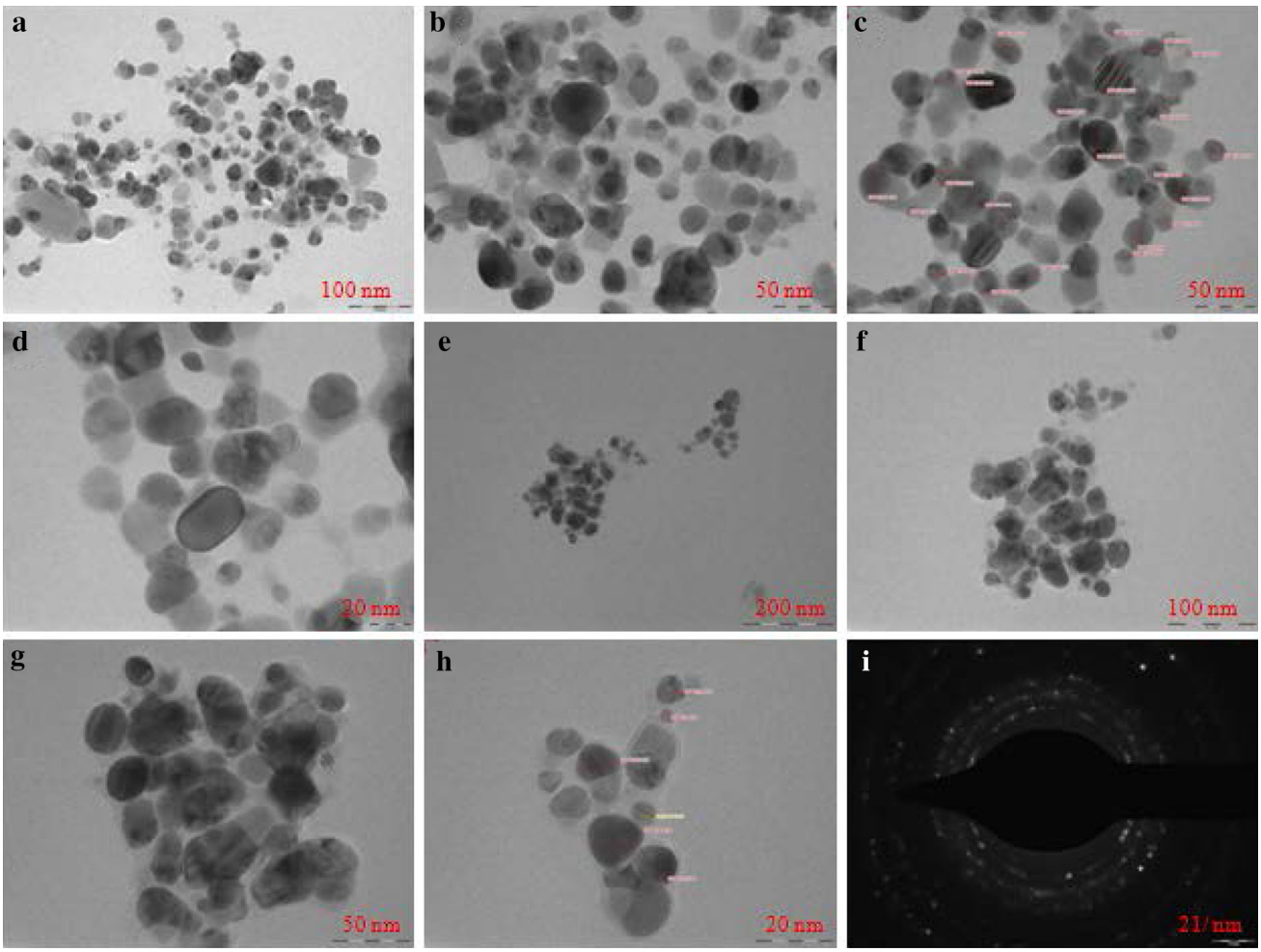

Fig. 5 TEM images of AgNPs at different magnification **a**–**d** in the presence of sunlight, **e**–**h** in the absence of sunlight, **i** SAED pattern of AgNPs in the presence of sunlight

behavior is due to the diffusion of nanoparticles into the bacteria resulting in the damage of cell membrane [55]. Another possibility recommended is the release of Ag^{+} ions from the nanoparticles, which enhance the bactericidal properties of nanoparticles [56].

The extract and AuNPs have no activity against the tested bacteria, but AgNPs show desirable results. The maximum zone of inhibition for AgNPs is shown by Gram-negative bacteria, *S. paratyphi*, (17 mm), in comparison to Gram-positive bacteria such as *P. aeroginosa* (15 mm), *S. pyogenes* (11 mm) and *S. faecalis* (14 mm) (Figure S8), which may be explained by the fact that the cell wall of the gram-positive bacteria is made of thick peptidoglycan layer consisting of linear polysaccharide chains cross linked by short peptides, thus forming more rigid structure leading to difficult diffusion of AgNPs compared to the Gram-negative bacteria where the cell wall has been composed of thinner peptidoglycan layer [57].

Evaluation of photo degradation

To see the potential application of biosynthesized Ag and AuNPs for environmental remediation, the degradation of two different cationic dyes (MG and MB) is studied at neutral condition ($\sim$pH 6). The experiments are carried out over period of 3 h both in the presence and absence of sunlight.

Degradation of malachite green

The change in the UV–Vis spectra of MG during the photodegradation process is given in Fig. 10b. Typically MG solutions display maximum absorbance at 315, 425, and 618 nm [58]. In the present study, the aqueous solution of MG solution has peaks at 316, 424 and 617 nm and the decrease in intensity of the major peak at 617 nm was monitored with time. In the absence of sunlight, the

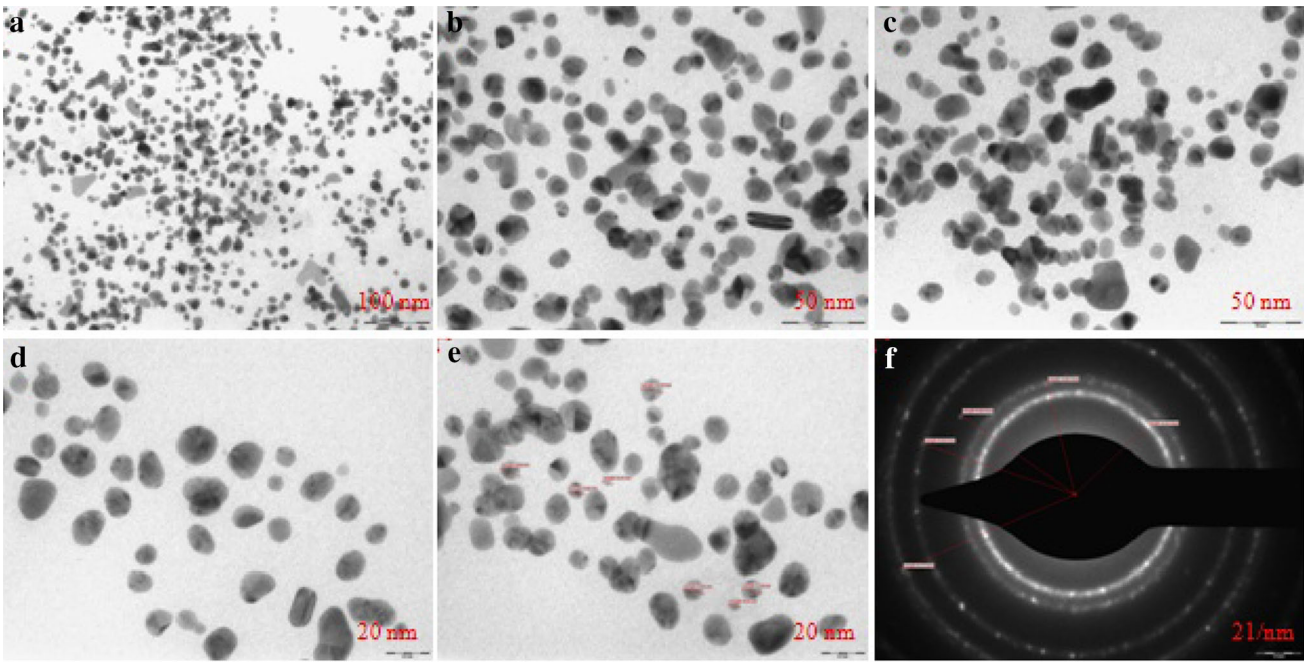

Fig. 6 **a–e** TEM images of AuNPs at different magnification and **f** SAED pattern

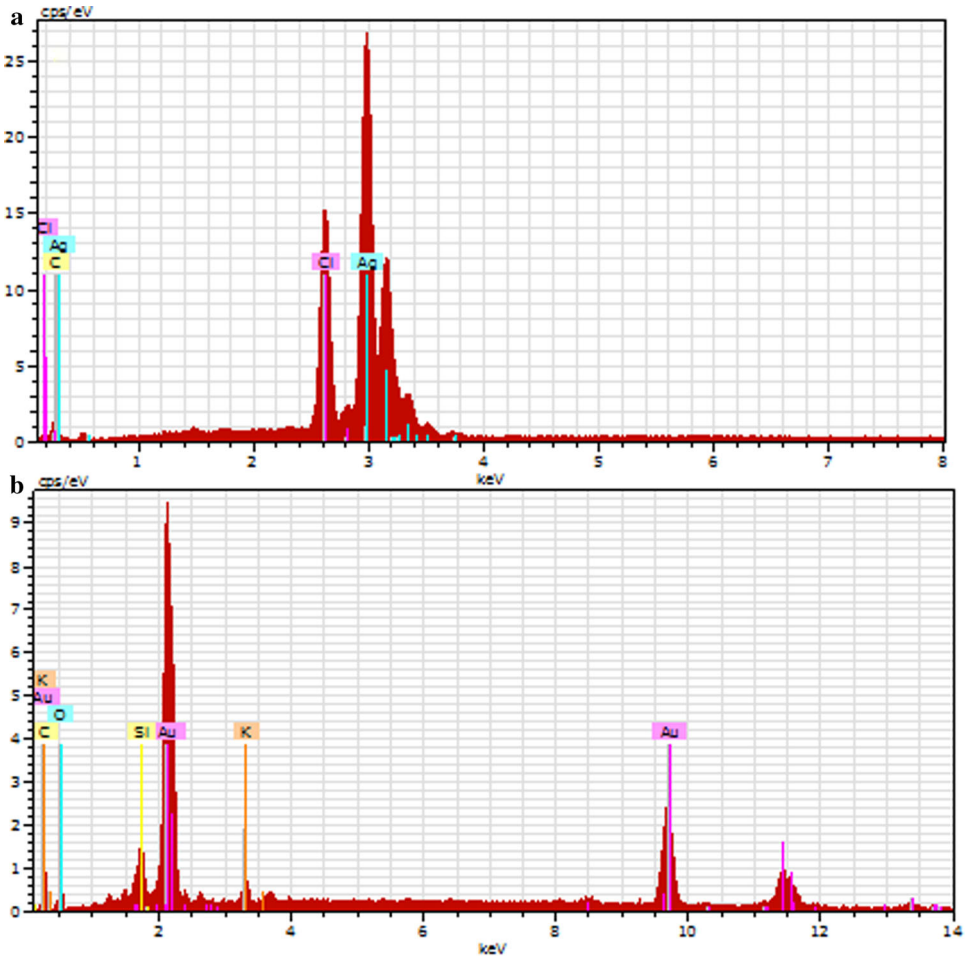

Fig. 7 EDAX spectra of **a** AgNPs and **b** AuNPs

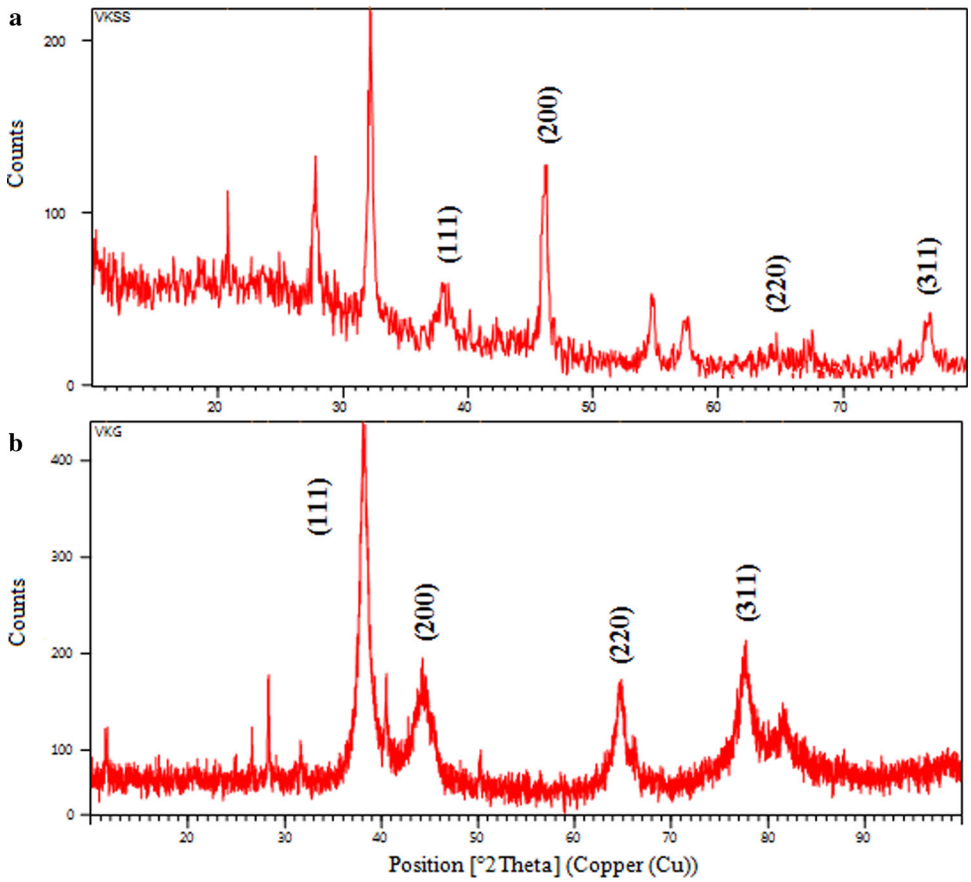

Fig. 8 XRD patterns of **a** AgNPs and **b** AuNPs

intensity of characteristic absorption band at 617 nm is decreased slowly (from 1.17 to 0.49 au in 180 min), corresponds to 57 % dye removal, but no shift in the λ_{max} is observed. During sunlight irradiation, the absorbance is decreased quickly (from 1.15 to 0.07 au in 180 min), which corresponds to 94 % removal of dye with a blue shift in λ_{max} (617–570 nm). No new absorption band is appeared around 255 nm indicating no leuco form of the dye is formed during the course of the reaction [59]. The plot of $-\ln(C/C_0)$ versus time is a straight line in both cases and the slope is equal to the rate of degradation, which is 0.38×10^{-2} and 1.51×10^{-2} min^{-1} in the absence and presence of sunlight, respectively. The fourfold increase in rate of the degradation in sunlight indicates the strong influence of sunlight on the reaction.

Another observation in the UV–vis spectra of MG is the initial decrease in the peak intensity at 617 nm (Fig. 10a, b). This may be due to the initial adsorption of MG over AgNPs [57]. From the decrease in initial peak intensity, the percentage adsorption of MG on the AgNPs is approximately 18 and 9.6 % in the absence and presence of sunlight, respectively. The less percentage of adsorption in the sunlight reaction may be due to the fact that the degradation of MG starts as soon as the adsorption takes place and the mechanism of this reaction is different.

The chemical structure of MG varies with solution pH. Chromatic MG^+ exists between the pH of 3.5–5.0 ($\lambda_{max} = 617$ nm), the protonated species MGH^+ exists below pH 2 ($\lambda_{max} = 255$ nm) and at pH value above 8 it is colorless due to the formation of carbinol base [56]. To see the effect of pH on degradation of MG, the reaction is also studied at pH 9 (Figure S9). At pH 9 the intensity of the peak at 617 nm is decreased immediately after the addition of NaOH (1.14–0.71 au) and 0.71–0.30 within 5 min after that it decreased gradually. A new peak is also observed at 252 nm, which may be due to the alkali fading of dye (leuco form) [59]. The fact that, no additional peak is noticed around 255 nm and the λ_{max} is shifted from 617 to 570 nm in the sunlight irradiated reaction suggests that the dye undergo degradation in the presence of sunlight rather than simple adsorption [60].

Further to substantiate the degradation, the FT-IR spectra of the dye before and after treating with AgNPs were recorded. In the case of pure MG, the FT-IR spectrum (Figure S10b) exhibits peaks at 2924, 1585, 1371, 1170 and 723 cm^{-1}. The peaks at 2924 cm^{-1} is assigned to

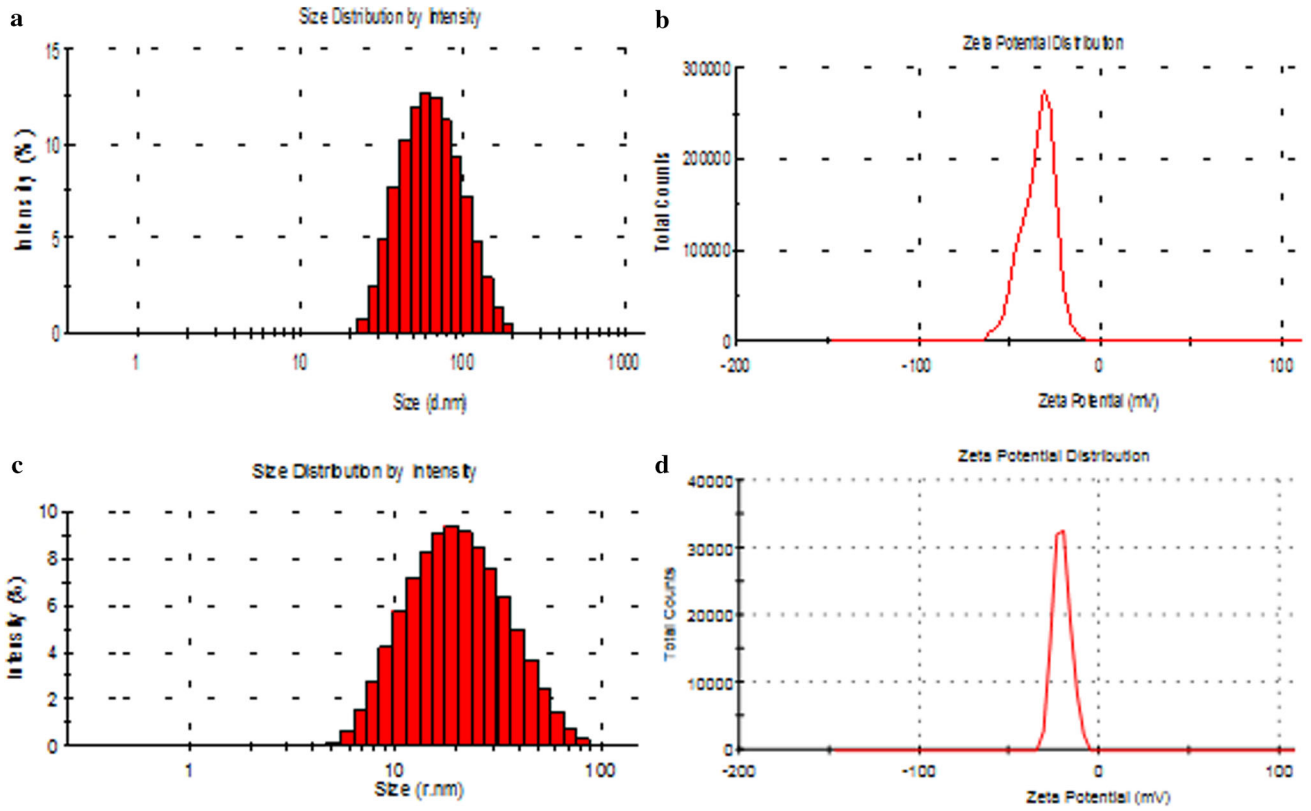

Fig. 9 Size distribution of **a** AgNPs; **c** AuNPs and Zeta potential of **b** AgNPs; **d** AuNPs

asymmetric C–H stretching of CH_3 group, the peak at 1585 cm^{-1} is assigned to C=C stretching of the benzene ring, the peak at 1170 cm^{-1} is due to C-N stretching vibration, the peak at 1371 cm^{-1} is assigned to stretching of $-CH_3/-CH_2$ and the peak at 725 cm^{-1} indicates symmetric out of plane bending of the ring hydrogen [61].

The FT-IR spectrum of solid AgNPs (Figure S10a) separated from the reaction mixture after the sunlight exposed degradation of MG shows that some peaks of MG have disappeared, specifically the peaks at 1371 and 1170 cm^{-1}, assigned to $-CH_3/-CH_2$ and C–N stretching vibrations, inferring the cleavage of C–N bond in N-methyl group. This is further supported by the shifting of λ_{max} in the UV–vis spectra in the presence of sunlight (Fig. 10b).

Degradation of methylene blue

Typically aqueous solutions of MB display maximum absorbance at 246, 292, 612 and 664 nm [62]. The decrease in intensity of peak at 663 nm was monitored with time and the change in the UV–Vis spectra during the photo degradation process is illustrated in Fig. 11. In the absence of sunlight, the intensity of characteristic absorption band of dye at 663 nm is decreased slowly, after 120 min 72 % of dye is removed without any shift in the λ_{max}. The absorbance of dye is decreased from 0.71 to 0.19 au. During sunlight irradiation, the absorbance is decreased rapidly with a huge blue shift in λ_{max} (114 nm; 663–549 nm), and no new absorption band is observed. The absorbance is decreased quickly from 0.71 to 0.07 au corresponding to 90 % of removal of dye after 120 min of sunlight irradiation. The plot of $-\ln(C/C_0)$ versus time (Fig. 11d) is a straight line in both cases and the slope is equal to the rate of degradation, which is 0.75×10^{-2} and 1.72×10^{-2} min^{-1} in the absence and presence of sunlight, respectively, which is approximately 2.3-fold increase in sunlight reaction. No new peak is formed around 256 nm confirming the absence of leuco-methylene blue [63]. Another observation in the UV–Vis spectra is the sudden initial decrease in the peak intensity of MB at 663 nm (Fig. 11a, b). This may be due to the initial adsorption of MB over AgNPs. From the decrease in initial peak intensity, the percentage adsorption of MB on the AgNPs is approximately 28 and 33.8 % in the absence and presence of sunlight, respectively.

The FT-IR spectrum of AgNPs (Figure S11a) obtained after the sunlight exposed degradation of MB shows that some peaks have disappeared, specifically the peaks at 1489 and 1178 cm^{-1} both due to vibration of heterocyclic skeleton, indicating the cleavage of heterocyclic ring. Moreover, the peaks at 1350 cm^{-1} due to C–N stretching

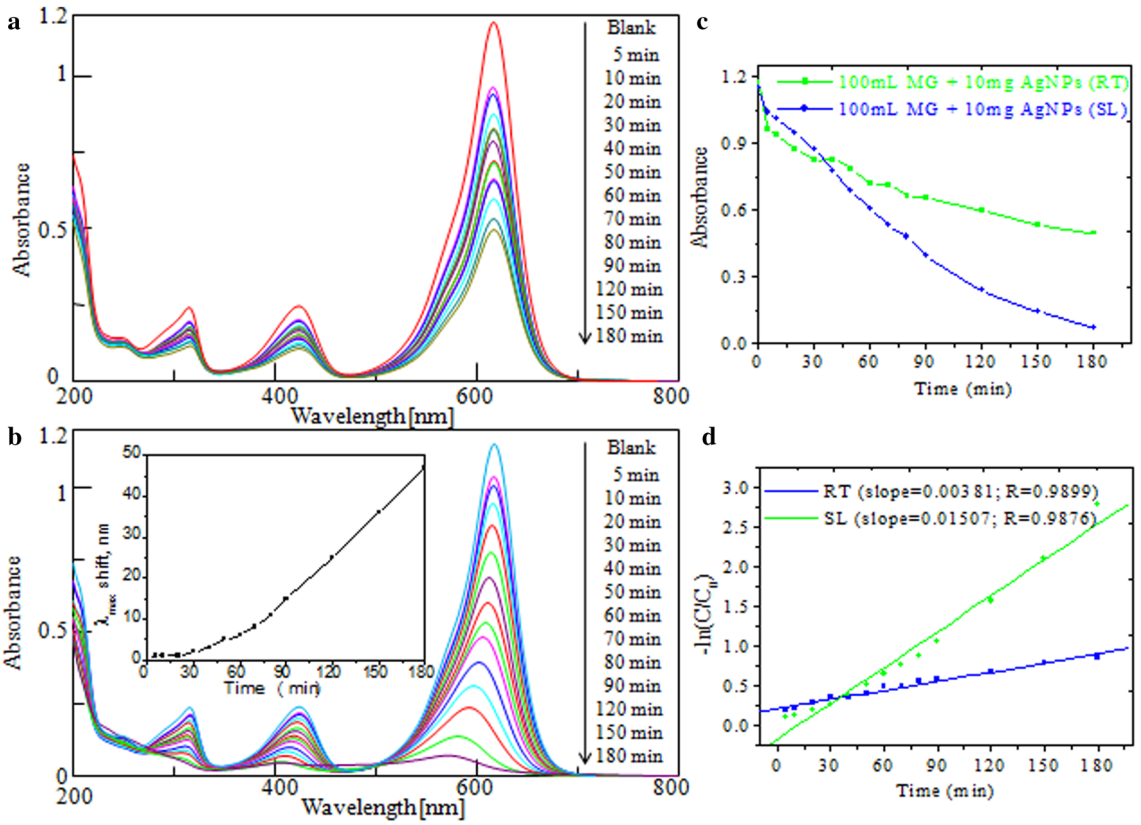

Fig. 10 UV–Vis spectra of MG as a function of time in the presence of AgNPs (MG—1×10^{-5} M, AgNPs-10 mg) **a** absence of sunlight, **b** presence of sunlight; *Inset*—shift in λ_{max} with time **c** plot of absorbance versus time and **d** plot of $-\ln(C/C_0)$ versus time

are also disappeared inferring the cleavage of C–N bond in N-methyl group. This is further supported by the large hypsochromic shift of λ_{max} in the UV–Vis spectrum in the presence of sunlight.

In the degradation of MB the intensity of LSPR band at 436 nm is increased with time both in the presence and absence of sunlight, but this trend is not observed in MG. After 90 min this peak spans entire visible region and no further decrease in intensity of peak at 663 nm is noticed even after 180 min although the blue color of MB is completely removed. This may be due to the interaction of AgNPs with dye molecules or any other intermediates formed during the reaction. The same trend was found in the recent articles and the authors attributed no reason [38, 39]. The intensity of peak at 246 nm decreased initially, after some time it started increasing in the reaction carried out in absence of light, but no such trend is observed in the light reaction. This may be due to interaction of AgNPs with adsorbed dye. The fact that this trend is not observed in light reaction means complete decomposition of intermediates containing phenothiazine moiety formed as a result of N-demethylation [64].

Parameters affecting dye degradation rate

Effect of dye concentration

The effect of concentration of MB (0.5, 1.0 and 2.0×10^{-5} M) was studied by keeping the catalyst dosage at 10 mg per 100 mL. While increasing the dye concentration from 0.5 to 1.0×10^{-5} M the rate of degradation also increases, but with further increase of concentration, the degradation rate decreases. This may be due to inability of light to reach the catalyst surface at high dye concentration [65]. The plot of $-\ln(C/C_0)$ versus time is a straight line (Figure S12). The same trend is observed in MG also.

Effect of catalyst dosage

The effect of catalyst dosage on the photocatalytic degradation of MB under sunlight was studied using different amounts of AgNPs (5, 10 and 15 mg per 100 mL) by keeping dye concentration constant (1×10^{-5} M). The degradation rate increases with increase of catalyst dosage (Figure S13). This may be due to an increased number of

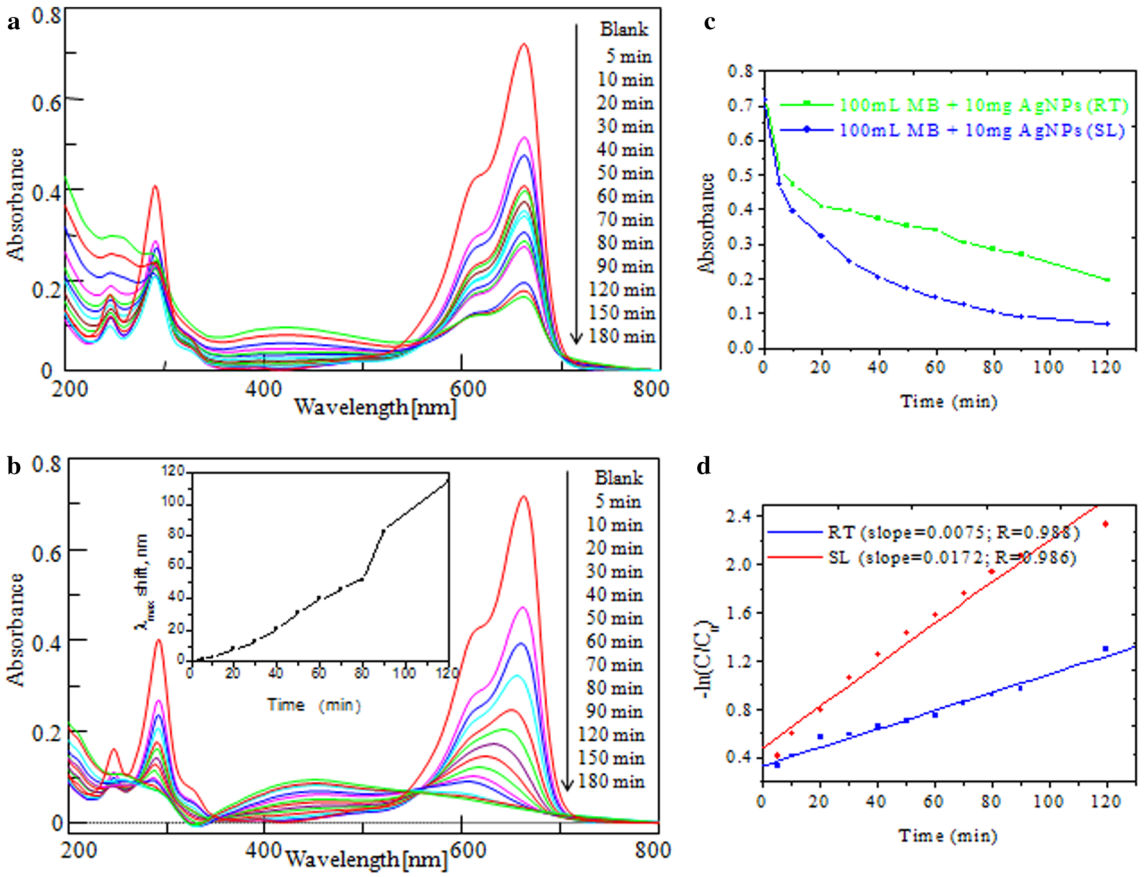

Fig. 11 UV–Vis spectra of MB as a function of time in the presence of AgNPs (MB—1 × 10^{-5} M, AgNPs—10 mg) **a** absence of sunlight, **b** presence of sunlight; *Inset*—shift in λ_{max} with time **c** plot of absorbance versus time and **d** plot of $-\ln(C/C_0)$ versus time

available adsorption and catalytic sites on the surface of the catalyst [66]. MG also shows the same trend.

Effect of pH

pH is one of the important parameters for study of dye degradation. The effect of pH on the degradation of dyes was studied at pH 4, 6 and 8 (pH 9 in the case of MG), which was maintained by adding 0.1 M H_2SO_4 or 0.1 M NaOH solution. At pH 4, degradation is less and at pH 8, degradation is high (Figures S14 and S15).

AuNPs could not be separated as solid by centrifugation and hence the degradation of MB and MG is studied in the presence of colloidal solutions of AuNPs. No appreciable degradation of the dye is noticed even after 3 h, may be due to the fact that the sunlight is insufficient to produce required electrons on the surface of AuNPs.

Mechanism for the degradation of dyes

Surfing chemical literature reveals that three possible mechanisms are proposed for the removal of the color of the dyes. 1. The dye may be converted to its leuco form by reduction or by increasing the pH [56]. 2. The dye may be adsorbed over the AgNPs, due to the high surface area of nanoparticles; large amount of dye can be removed. 3. The dye can be degraded on the surface of AgNPs due to hot electrons present on the surface created by the intraband transition of electrons (5sp) in the AgNPs due to the LSPR [67].

In this study the last mechanism seems to be operative (Fig. 12). The AgNPs prepared through biosynthetic route are negatively charged as supported by zeta potential (−34.9 mV). Initially the cationic dyes may get adsorbed over the AgNPs due to electrostatic interaction and due to proximity, the excited electrons may degrade the dye in the nanoparticles-adsorbate interface.

The blueshift in λ_{max} suggests the formation of N-demethylated intermediates in degradation pathway. The color of MB solutions becomes less intense (hypsochromic effect) when auxochromic groups (methyl or methylamine) are removed. For dyes containing auxochromic alkylamine groups, N-dealkylation plays an important role in photocatalytic degradation [68]. No new peaks for intermediates appeared during the degradation of both MG and MB and almost nil COD value after the reaction indicates the complete degradation of dyes in sunlight. Hence in the light reactions, it

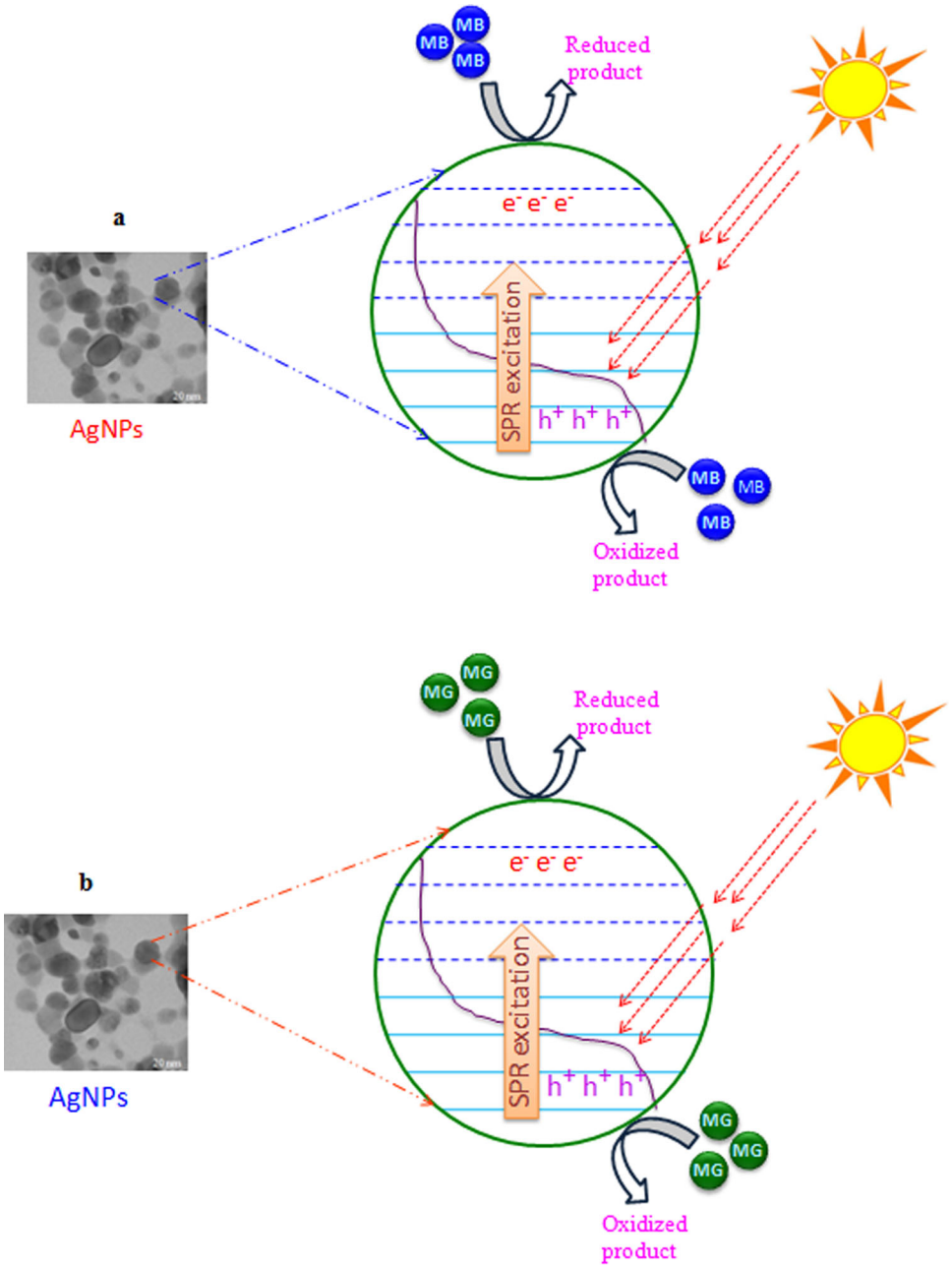

Fig. 12 Schematic diagram of photodegradation of **a** MB and **b** MG under sunlight irradiation over AgNPs

appears degradation takes place via demethylation process and in the absence of light the removal of color is due to adsorption. However, further research using other plasmonic nanoparticles is required to prove this mechanism.

Conclusions

H. asiatica leaves extract has been used as a reducing and capping agent for the photobiological synthesis of Ag and AuNPs. The formation of nanoparticles is observed by color change and confirmed by UV–Vis spectroscopy. Active water-soluble biomolecules such as glycosides and flavonoids from the extract are responsible for the reduction and also act as stabilizing agent against agglomeration of nanoparticles. From TEM, the average sizes of Ag and AuNPs are found to be 21 and 8 nm, respectively. Small quantity of AgNPs (0.1 g/L) has potential capacity to remove cationic dyes in the presence of sunlight and have noticeable antibacterial activity. Utilization of surface plasmonic resonance excitation of noble metal nanoparticles for various catalytic processes is the current field in green chemistry. Since in this reaction a plant is used as a reductant and stabilizer for preparing noble metal

nanoparticles and abundantly available sunlight is used to drive the photo degradation of dyes, this green route may be used for environmental remediation and in water treatment technology.

Acknowledgments This work is sponsored by UGC, New Delhi. One of the author, T. Akkini Devi thanks UGC for Project Fellowship. The authors express sincere thanks to the secretary, V.O.Chidambaram College, Tuticorin, India for providing necessary laboratory facilities. SAIF, IIT Bombay and DFRL, Mysore, India are acknowledged for TEM and DLS analysis.

References

1. Hiroki, H., Frank, E.O.: A simple large-scale synthesis of nearly monodisperse gold and silver nanoparticles with adjustable sizes and with exchangeable surfactants. Chem. Mater. **16**, 2509–2511 (2004)
2. Zhang, P., Chu, A.Y., Sham, T., Yao, Y., Lee, S.: Chemical synthesis and structural studies of thiol-capped gold nanoparticles. Can. J. Chem. **87**, 335–340 (2009)
3. Jack, B., Jeyanthinath, M., Annett, T., Erik, S.M., Umadevi, M.: Chemical synthesis of silver nanoparticles for solar cell applications. Phys. Status Solidi C **8**, 924–927 (2011)
4. Yasmeen, J., Baykal, A.: Sirajuddin.: green chemical synthesis of silver nanoparticles and its catalytic activity. J. Inorg. Organomet. Polym. **24**, 401–406 (2014)
5. Anjali, P.: Photochemical synthesis of gold nanoparticles via controlled nucleation using a bioactive molecule. Mater. Lett. **58**, 529–534 (2004)
6. Lilia, C.C., Flávia, R.O.S., Láercio, G.: A simple method to synthesize silver nanoparticles by photo-reduction. Colloids and surfaces A: physicochem. Eng. Aspects **305**, 54–57 (2007)
7. Huang, W., Chen, Y.: Photochemical synthesis of polygonal gold nanoparticles. J. Nanopart. Res. **10**, 697–702 (2008)
8. del Rodríguez-Torres, M.P., Luis, A.D., Pedro Salas, Claramaría, R.G., Martin O.: UV photochemical synthesis of heparin-coated gold nanoparticles. Gold Bull. **47**, 21–31 (2013)
9. Sun, X., Dong, S., Wang, E.: One-step synthesis and characterization of polyelectrolyte-protected gold nanoparticles through a thermal process. Polymer **45**, 2181–2184 (2004)
10. Jeevanandam, P., Srikanth, C.K.: Suchi Dixit.: synthesis of monodisperse silver nanoparticles and their self-assembly through simple thermal decomposition approach. Mater. Chem. Phys. **122**, 402–407 (2010)
11. Chaudhary, G.R., Singh, P., Kaur, G., Mehta, S.K., Kumar, S., Dilbaghi, N.: Multifaceted approach for the fabrication of metallomicelles and metallic nanoparticles using solvophobic bisdodecylamine palladium (II) chloride as precursor. Inorg. Chem. **54**, 9002–9012 (2015)
12. Sakamoto, M., Fujistuka, M., Majima, T.: Light as a construction tool of metal nanoparticles: synthesis and mechanism. J. Photochem. Photobiol. C **10**, 33–56 (2009)
13. Morones, J.R., Elechiguerra, J.L., Camacho, A., Ramirez, J.T.: The bactericidal effect of silver nanoparticles. Nanotechnology **16**, 2346–2353 (2005)
14. Gajbhiye, M., Kesharwani, J., Avinash, I., Aniket, G., Rai, M.: Fungus-mediated synthesis of silver nanoparticles and their activity against pathogenic fungi in combination with fluconazole. Nanomed. Nanotech. Biol. Med. **5**, 382–386 (2009)
15. Javed, M., Dwivedi, S., Braj, R.S., Al-Khedhairy, A.A., Ameer, A., Alim, N.: Production of antimicrobial silver nanoparticles in water extracts of the fungus *Amylomyces rouxii*s train KSU-09. Bioresour. Tech. **101**, 8772–8776 (2010)
16. Kumar, R., Roopan, S.M., Prabhakarn, A., Venkatesan, G.K., Chakroborty, S.: Agricultural waste *Annona squamosa* peel extract: biosynthesis of silver nanoparticles. Spectrochim. Acta Part A **90**, 173–176 (2012)
17. Kouvaris, P., Delimitis, A., Zaspalis, V., Papadopoulos, D., Tsipas, S.A., Nikolaos, M.: Green synthesis and characterization of silver nanoparticles produced using *Arbutus unedo* leaf extract. Mater. Lett. **76**, 18–20 (2012)
18. Amaladhas, T.P., Sivagami, S., Akkini Devi, T., Ananthi, N., Priya Velammal, S.: Biogenic synthesis of silver nanoparticles by leaf extract of *Cassia angustifolia.* Adv. Nat. Sci.: Nanosci. Nanotechnol. **3**, 1–7 (2012)
19. Gogoi, K., Saikia, J.P., Konwar, B.K.: Immobilizing silver nanoparticles (SNP) on *Musa balbisiana* cellulose. Colloids Surf. B **102**, 136–138 (2013)
20. Kathiresan, K., Alikunhi, N.M., Manickaswami,G., Nabikhan, A., Gopalakrishnan, A.: Synthesis of silver nanoparticles by coastal plant *Prosopis chilensis* (L.) and their efficacy in controlling vibriosis in shrimp *Penaeus monodon*. Appl. Nanosci. **3**, 65–73 (2013)
21. Edison, T.N.J.I., Sethuraman, M.G.: Electrocatalytic reduction of benzyl chloride by green synthesized silver nanoparticles using pod extract of *Acacia nilotica*. ACS Sustain. Chem. Eng. **1**, 1326–1332 (2013)
22. Shankar, S.S., Rai, A., Ahmad, A., Sastry, M.: Controlling the optical properties of lemongrass extract synthesized gold nanotriangles and potential application in infrared-absorbing optical coatings. Chem. Mater. **17**, 566–572 (2005)
23. Das, R.K., Sharma, P., Nahar, P., Bora, U.: Synthesis of gold nanoparticles using aqueous extract of *Calotropis procera* latex. Mater. Lett. **65**, 610–613 (2011)
24. Aswathy, A.S., Philip, D.: Green synthesis of gold nanoparticles using *Trigonella foenum-graecum* and its size-dependent catalytic activity. Spectrochim. Acta Part A Mol. Biomol. Spectrosc. **97**, 1–5 (2012)
25. Dash, S.S., Rakhi, M., Arun, K.S., Braja, G.B., Patra, B.K.: *Saraca indica* bark extract mediated green synthesis of poly shaped gold nanoparticles and its application in catalytic reduction. Appl. Nanosci. **4**, 485–490 (2014)
26. Sujitha, M.V., Kannan, S.: Green synthesis of gold nanoparticles using *Citrus* fruits (*Citrus limon*, *Citrus reticulata* and *Citrus sinensis*) aqueous extract and its characterization. Spectrochim. Acta Part A Mol. Biomol. Spectrosc. **102**, 15–23 (2013)
27. Nishant, S., Mausumi, M.: Biosynthesis and characterization of gold nanoparticles using *zooglearamigera* and assessment of its antibacterial property. J Clust Sci. **26**, 675–692 (2015)
28. Rajasekharreddy, P., Pathipati, U.R., Bojja, S.: Qualitative assessment of silver and gold nanoparticles synthesis in various plants: a photobiological approach. J. Nanopart. Res. **12**, 1711–1721 (2010)
29. Rastogi, L., Arunachalam, J.: Sunlight based irradiation strategy for rapid green synthesis of highly stable silver nanoparticles using aqueous garlic (*Allium sativum*) extract and their antibacterial potential. Mater. Chem. Phys. **129**, 558–563 (2011)
30. Zarchi, A.A.K., Mokhtari, N., Arfan, M., Rehman, T., Ali, M., Amini, M., Majidi, R.F., Shahverdi, A.R.: A sunlight-induced

method for rapid biosynthesis of nanoparticles using an *Andrachnea chordifolia* ethanol extract. Appl. Phys. A **103**, 349–353 (2011)
31. Pathipati, U.R., Rajasekharreddy, P.: Green synthesis of silver-protein (core–shell) nanoparticles using *Piper betle* L. leaf extract and its ecotoxicological studies on *Daphnia magna*. Colloids Surf. A: Physicochem. Eng. Asp. **389**, 188–194 (2011)
32. Xuetuan, W., Mingfang, L., Li, W., Yang, L., Liang, X., Xu, L., Peng, K., Liu, H.: Synthesis of silver nanoparticles by solar irradiation of cell-free *Bacillus amyloliquefaciens* extracts and $AgNO_3$. Bioresour. Tech. **103**, 273–278 (2012)
33. Amaladhas, T.P., Usha, M., Naveen, S.: Sunlight induced rapid synthesis and kinetics of silver nanoparticles using leaf extract of *Achyranthes aspera* L. and their antimicrobial applications. Adv. Mat. Lett. **4,** 779–785 (2013)
34. Luo, Y.: Size-controlled preparation of dendrimer-protected gold nanoparticles: a sunlight irradiation-based strategy. Mater. Lett. **62**, 3770–3772 (2008)
35. Pienpinijtham, P., Han, X.X., Suzuki, T., Thammacharoen, C., Ekgasit, S., Ozaki, Y.: Micrometer-sized gold nanoplates: starch mediated photochemical reduction synthesis and possibility of application to tip-enhanced Raman scattering (TERS). Phys. Chem. Chem. Phys. **14**, 9636–9641 (2012)
36. Jebakumar, I.E.T., Sethuraman, M.G.: Instant green synthesis of silver nanoparticles using *Terminalia chebula* fruit extract and evaluation of their catalytic activity on reduction of methylene blue. Process Biochem. **47**, 1351–1357 (2012)
37. Vidhu, V.K., Philip, D.: Catalytic degradation of organic dyes using biosynthesized nanoparticles. Micron **56**, 54–62 (2014)
38. Vanaja, M., Paulkumar, K., Baburaja, M., Rajeshkumar, S., Gnanajobitha, G., Malarkodi, C., Sivakavinesan, M., Annadurai, G.: Degradation of methylene blue using biologically synthesized silver nanoparticles. Bioinorg. Chem. Appl. **2014**, 1–8 (2014)
39. Suvith, V.S.: Daizy Philip: catalytic degradation of methylene blue using biosynthesized gold and silver nanoparticles. Spectrochim. Acta Part A Mol. Biomol. Spectrosc. **118**, 526–532 (2014)
40. Hemant, P.B., Patil, C.D., Salunkhe, R.B., Suryawanshi, R.K., Salunke, B.K., Patil, S.V.: Transformation of aromatic dyes using green synthesized silver nanoparticles. Bioprocess Biosyst. Eng. **37**, 1695–1705 (2014)
41. Sinha, T., Ahmaruzzaman, M.: A novel green and template free approach for the synthesis of gold nanorice and its utilization as a catalyst for the degradation of hazardous dye. Spectrochim. Acta Part A Mol. Biomol. Spectrosc. **142**, 266–270 (2015)
42. Srinath, B.S, Ravishankar Rai, V.: Biosynthesis of gold nanoparticles using extracellular molecules produced by *Enterobacter aerogenes* and their catalytic study. J. Clust Sci. **26**, 1483–1494 (2015)
43. Matsuda, H., Morikawa, T., Ueda, H., Yoshikawa, M.: Medicinal Foodstuffs. XXVII. (1) Saponin Constituents of Gotu Kola (2): structures of New Ursane- and Oleanane-Type Triterpene Oligoglycosides, Centellasaponins B, C, and D, from *Centella asiatica* Cultivated in Sri Lanka. Chem. Pharm. Bull. **49**, 1368–1371 (2001)
44. Subathra, M., Shila, S., Devi, M.A., Panneerselvam, C.: Emerging role of *Centella asiatica* in improving age-related neurological antioxidant status. Exp. Geront. **40**, 707–715 (2005)
45. Kavitha, D., Namasivayam, C.: Experimental and kinetic studies on Methylene blue adsorption by coir pith carbon. Bioresour. Technol. **98**, 14–21 (2007)
46. Srivastava, S., Sinha, R., Roy, D.: Toxicological effects of malachite green. Aquat. Toxicol. **66**, 319–329 (2004)
47. Kang, S.F., Liao, C.H., Po, S.T.: Decolorization of textile wastewater by photo-fenton oxidation technology. Chemosphere **41**, 1287–1294 (2000)
48. Sheny, D.S., Joseph, M., Daizy, P.: Phytosynthesis of Au, Ag and Au–Ag bimetallic nanoparticles using aqueous extract and dried leaf of *Anacardium occidentale*. Spectrochim. Acta Part A **79**, 254–262 (2011)
49. Venkatesh, G., Kalpana, U., Prasad, M.N.V., Rao, N.V.S.: Green synthesis of gold and silver nanoparticles using *Achyranthes aspera* L. leaf extract. Adv. Sci. Eng. Med. **4**, 1–6 (2012)
50. ShahirJamil, S., Nizami, Q., Salam, M.: *Centella asiatica* (Linn.) óA Review. Natural Product Radiance **6**, 158–170 (2007)
51. Satheesh Kumar, B., Suchethakumari, N., Vadisha, S.B., Sharmila, K.P., Mahesh Prasad, B.: Preliminary phytochemical screening of various extracts of Punica granatum peel, whole fruit and seeds. Nitte Univ. J. Health Sci. **4**, 34–38 (2012)
52. Magudapathy, P., Gangopadhyay, P., Panigrahi, B.K., Nair, K.G.M., Dhara, S.: Electrical transport studies of Ag nanoclusters embedded in glass matrix. Phys. B **299**, 142–146 (2001)
53. Narayanan, K.B., Sakthivel, N.: Facile green synthesis of gold nanostructures by NADPH-dependent enzyme from the extract of *Sclerotium rolfsii*. Colloids Surf. A Physicochem. Eng. Asp. **380**, 156–161 (2011)
54. Wani, I.A., Aparna, G., Ahmed, J., Ahmad, T.: Silver nanoparticles: ultrasonic wave assisted synthesis, optical characterization and surface area studies. Mater. Lett. **65**, 520–522 (2011)
55. Panacek, A., Kvitek, L., Prucek, R., Kolar, M., Vecerova, R., Pizurova, N.: Silver colloid nanoparticles: synthesis, characterization, and their antibacterial activity. J. Phys. Chem. B **110**, 16248–16253 (2006)
56. Kim, K.J., Sung, W.S., Suh, B.K., Moon, S.K., Choi, J.S., Kim, J.G.: Antifungal activity and mode of action of silver nanoparticles on *Candida albicans*. Biometals **22**, 235–242 (2009)
57. Shrivastava, S., Bera, T., Roy, A., Singh, G., Rao, P.R., Dash, D.: Characterization of enhanced antibacterial effects of novel silver nanoparticles. Nanotechnology **18**, 225103–225111 (2007)
58. Ouarda, M., Oualid, H., Christian, P.: Sonochemical degradation of malachite green in water. Chem. Eng. Prog. **62**, 47–53 (2012)
59. Lee, Y.C., Kim, J.Y., Shin, H.J.: Removal of malachite green (MG) from aqueous solutions by adsorption, precipitation, and alkaline fading using talc. Sep. Sci. Technol. **48**, 1093–1101 (2013)
60. Han, H.T., Khan, M.M., Kalathil, S., Lee, J., Cho, M.H.: Simultaneous enhancement of methylene blue degradation and power generation in microbial fuel cell by gold nanoparticles. Ind. Eng. Chem. Res. **52**, 8174–8181 (2013)
61. Ganesh, P., Satish, K., Ganesh, S., Sanjay, G.: Biodegradation of malachite green by *Kocuria rosea* MTCC 1532. Acta Chim. Slov. **53**, 492–498 (2006)
62. Sonal, S., Rimi, S., Charanjit, S., Bansa, S.: Enhanced photocatalytic degradation of methylene blue using $ZnFe_2O_4$/MWCNT composite synthesized by hydrothermal method. Indian J. Mater. Sci. **2013**, 1–6 (2013)
63. Impert, O., Katafias, A., Kita, P., Mills, A., Pietkiewicz-Graczyk, A., Wrzeszcz, G.: Kinetic and mechanism of fast leuco-methylene blue oxidation by copper (II)-halide species in acidic aqueous media. Dalton Trans. (2003). doi:10.1039/B205786G
64. Zhang, T., Oyama, T., Aoshima, A., Hidaka, H., Zhao, J., Serpone, N.: Photooxidative demethylation of methylene blue in aqueous TiO_2 dispersions under UV irradiation. J. Photochem. Photobiol. A Chem. **140**, 163–172 (2001)
65. Sivakumar, P., Gaurav Kumar, G.K., Sivakumar, P., Renganathan, S.: Synthesis and characterization of ZnS-Ag nanoballs and its application in photocatalytic dye degradation under visible light. J. Nanostruct. Chem. (2014). doi:10.1007/s40097-014-0107-0
66. Hashemzadeh, F., Rahimin, R., Ghaffarinejad, A.: Mesoporous nanostructures of Nb2O5 obtained by an EISA route for the treatment of malachite green dye-contaminated aqueous solution

under UV and visible light irradiation. Ceram. Int. **40**, 9817–9829 (2014)
67. Sarina, S., Waclawik, E.R., Zhu, H.: Photocatalysis on supported gold and silver nanoparticles under ultraviolet and visible light irradiation. Green Chem. **15**, 1814–1833 (2013)
68. Liu, Y., Yu, H.B., Zhan, S.H., Li, Y.L.Z.N., Yang, X.Q.: Fast degradation of Methylene Blue with electrospun hierarchical-Fe_2O_3 nanostructured fibers. J. Sol–Gel. Sci. Technol. **58**, 716–723 (2011)